JOURNAL OF PROPULSION AND POWER
Vol. 13, No. 5, September–October 1997

Performance and Acceleration Process of Quasisteady Magnetoplasmadynamic Arcjets with Applied Magnetic Fields

Hirokazu Tahara,* Yoichi Kagaya,† and Takao Yoshikawa‡
Osaka University, Toyonaka, Osaka 560, Japan

A quasisteady magnetoplasmadynamic (MPD) arcjet with an applied magnetic field was investigated to improve the thruster performance and understand the complex acceleration mechanisms with both the self-induced and applied magnetic fields. The MPD arcjet was operated with hydrogen, a mixture of nitrogen and hydrogen simulating hydrazine, and argon at discharge currents of 3–18 kA in high specific impulse levels around a critical discharge current predicted from the rules of Alfvén's ionization velocity or minimum input power. The application of axial magnetic fields achieved higher thrust efficiencies than those for only the self-induced magnetic field at constant specific impulses, and still achieved stable operations at higher specific impulses with less electrode erosion. The following guidelines were suggested to achieve higher thruster performance: 1) the axial magnetic field strength must be smaller than the azimuthal self-field strength in the main discharge region near the cathode tip, and 2) the applied magnetic field lines must expand gradually downstream for smooth expansion of plasma. Furthermore, the measured pressures on the electrodes and the current distributions in the discharge chamber showed that the overall thrust measured by a pendulum method increased, in spite of a decrease in the electromagnetic pumping thrust and a small contribution of Hall acceleration. Thus, an additional thrust component because of the axial magnetic field, such as that caused by swirl acceleration, is expected to exist.

Nomenclature

B = magnetic field
b = self-field electromagnetic thrust coefficient
e = electron charge
g = standard acceleration of gravity
I_{sp} = specific impulse
J = discharge current or current
J_c = analytically predicted critical operational current
J^* = limiting operational current
j = current density
M = ion mass
$\dot{m}$ = mass flow rate
P_{th} = theoretical radial equilibrium pressure on the cathode
r = radius
T = thrust
T_m = theoretical electromagnetic thrust caused by azimuthal self-induced magnetic field
T_p = ratio of thrust to input power
U_c = Alfvén's critical ionization velocity
V = discharge voltage
α = fraction of current entering the cathode tip to discharge current
η = thrust efficiency
μ = permeability in free space
Φ = propellant dissociation and ionization voltage

Subscripts
a = anode
c = cathode
r, θ, z = cylindrical coordinates

Received Dec. 1, 1995; revision received March 12, 1997; accepted for publication May 5, 1997.

*Associate Professor, Department of Mechanical Engineering, Faculty of Engineering Science, 1-3, Machikaneyama, Member AIAA.
†Assistant Engineer, Department of Mechanical Engineering, Faculty of Engineering Science, 1-3, Machikaneyama.
‡Professor, Department of Mechanical Engineering, Faculty of Engineering Science, 1-3, Machikaneyama. Member AIAA.

Introduction

A QUASISTEADY magnetoplasmadynamic (MPD) arcjet characterized by high specific impulse and large thrust density is a reaction force device suitable for a future thruster in space.[1] Quasisteady applied-field MPD arcjets have been investigated to improve the thruster performance at specific impulse levels of 1000–2000 s for near-Earth missions.[2–5] The efficient acceleration caused by thermalization enhanced by axial magnetic fields is expected for hydrogen or ammonia propellant with large mass flow rates, and the thrust efficiency and the thrust-to-power ratio reached 42% and 52 mN/kW, respectively, with hydrogen. This paper describes current research on thruster performance and acceleration mechanisms of a quasisteady MPD arcjet with applied magnetic fields at high specific impulse levels around a limiting discharge current.[6,7]

Self-field MPD thruster performance is improved by increasing the discharge current for a given mass flow rate. However, the maximum current may be limited by the onset phenomenon; that is, the thruster operation may become unacceptable because of significant electrode erosion and discharge voltage fluctuations at a certain limit of the discharge current, resulting in a maximum attainable specific impulse.[8] In the present study, under axial-field application, the limiting current J^* is determined from the discharge voltage waveform, and it is compared with a critical current J_c, which is analytically derived from the theories of Alfvén's critical speed and self-field electromagnetic acceleration.[8–11] The anomalous features above the limiting current may be related to anode instability because of the shortage of current carrier, although the physical processes are still poorly understood.

When MPD thrusters were operated in a steady-state mode at low current levels below 3 kA, in the 1960s, axial magnetic fields were applied in the discharge chambers with heavy solenoidal coils for progressive improvement of the thrust

characteristics.[9-12] Axial-field application seems to be unattractive for space application because of the excessive magnetic coil's weight, extra power, and degrading the simplicity of the self-field thruster. From practical utility, we used a particular method to remove the penalties; i.e., a few-turn coils that are located outside the annular anode, are connected in series with a main discharge circuit of a pulse forming network (PFN).[2-6] In this scheme, the applied magnetic field strength increases linearly with the discharge current. Recently, Myers[13,14] studied the effects of electrode geometry and applied magnetic field strength on MPD thruster performance to establish a scaling law of steady-state applied-field MPD thrusters with argon and hydrogen propellants at input power levels around 100 kW. In his experimental conditions,[13,14] swirl acceleration was expected to be mainly dominant, although the performance characteristics were intensively modified by changes of electrode geometry or the existence of a magnetized sheath on the anode. Sasoh and Arakawa[15] investigated a steady-state applied-field MPD thruster with hydrogen, helium, nitrogen, and argon at input powers of 2–16 kW. With lower mass flow rates, they concluded that the main thrust production was because of Hall acceleration. They still analytically derived a thrust formula of applied-field MPD thrusters from the idealized energy conservation equation.[16] The thrust formula roughly estimated thrust components caused by swirl, Hall, and self-field accelerations. It qualitatively explained the change of a main thrust production mechanism with varying operational condition. These successful results will be useful for the optimum design of applied-field MPD thruster chambers at some operational conditions with a much higher applied magnetic field strength than the self-field strength. However, few comments are given to the present study at experimental conditions with both the self-induced and applied magnetic fields, in which axial magnetic fields are applied in MPD discharge chambers with strong azimuthal self-induced magnetic fields.

In the present study, the effect of axial magnetic fields on quasisteady MPD thruster performance in the high specific impulse range is examined, using hydrogen, a mixture of nitrogen and hydrogen-simulating hydrazine, and argon. Furthermore, pressures on the electrodes and current densities in the discharge chamber are measured to understand the inner discharge features and the complex acceleration processes with both the azimuthal magnetic field induced by the discharge current and the applied axial magnetic field.

Experimental Apparatus

Figure 1 shows the cross section of the quasisteady MPD arcjet with applied magnetic fields used for the present study. The arcjet, which is called the MY-III arcjet, is provided with a straight-diverging anode made of copper.[2-7] The anode nozzle's exit diameter is 58 mm, and it has a 20-deg half-angle. The anode is divided azimuthally into four parts; the slits between them are filled with electrically insulating and heat-resisting ceramics. The azimuthal eddy current induced on the anode surface is cut by this method, and pulsed magnetic fields can penetrate quickly into the discharge chamber. A cylindrical cathode 17.5 mm in length and 9.5 mm in diameter is made of thoriated tungsten. The MY-III arcjet is equipped with ring coils connected in series with the PFN for application of axial magnetic fields. The rise time of the applied magnetic fields in the discharge chamber was confirmed to be the same as that of the discharge current with a magnetic probe.

Propellants are injected with a cathode/anode slit ratio of 50/50 into the discharge chamber through a fast-acting valve (FAV) fed from a high-pressure reservoir. The rise time and width of the gas pulse, measured with a fast ionization gauge, are 0.5–1.0 and 6 ms, respectively. The mass flow rates are controlled by adjustment of the reservoir pressure and the orifice diameter of the FAV.

The power-supplying PFN, which is capable of storing 62 kJ at 8 kV, delivers a single nonreversing quasisteady current of a maximum of 27 kA, with a pulse width of 0.6 ms. Because the gas pulse width is much longer than the discharge current pulse width, the present MPD arcjet operational system is not optimized. The influence of the magnetic coils in series with the PFN on the discharge circuit itself can be neglected because of the very small inductance of the coils. Discharge currents are measured by a Rogowski coil calibrated with a known shunt resistance. Voltage measurement is performed with a current probe (Iwatsu CP-502), which detects the small current bled through a known resistor (10 kΩ) between the electrodes. A vacuum tank 5.75 m in length and 0.6 m in diameter, where the arcjet is fired, is evacuated to 10^{-3} Pa prior to each discharge.

Applications of External Magnetic Fields

Because axial magnetic fields are applied with a few turn coil in series with the PFN, the field strength is proportional to the discharge current. In this study, two types of axial magnetic fields are used, and they are called the C1L- and C2L-type fields.[2-6] Calculated magnetic field lines, field intensities, and locations of the coils at 10 kA are shown in Fig. 2. The C1L-type field consists of a one-turn coil at a radius of 57 mm and an axial position 14 mm downstream of the cathode tip. The C2L-type field is composed of a two-turn coil at the same location as that of the C1L-type field. Therefore, the C2L-type field is twice the applied field strength of the C1L-type field,

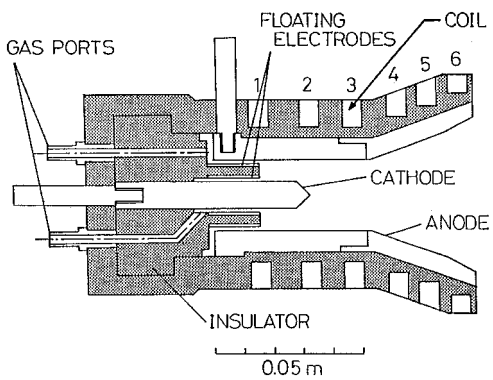

Fig. 1 Cross section of a quasisteady MY-III magnetoplasmadynamic arcjet with applied magnetic fields.

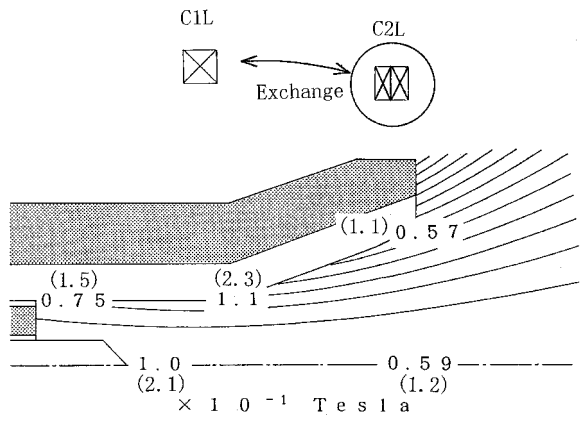

Fig. 2 Calculated intensities and profiles of applied magnetic fields in series with pulse-forming network at 10 kA. The C1L- and C2L-type fields consist of one- and two-turn coils, respectively. The values in parentheses are magnetic field intensities for the C2L-coil-type field.

although both field shapes are the same. The azimuthal self-field intensities, which are measured with a $\dot{B}_\theta$ probe, at 10 kA for a mixture of $N_2 + 2H_2$, are about $0.18T$ near the cathode tip and about $0.03T$ at the nozzle end. For the C1L-type field, the axial magnetic field strength near the cathode tip, where intensive heating occurs, is lower than that for only the self-induced magnetic field, regardless of discharge currents and gas species, although the field strength for the C2L-type field is higher. On the other hand, the axial field intensities near the nozzle end are lower than the self-field intensities for both coil types.

Thrust Measurement

Thrust is measured by a pendulum method. The MPD arcjet and FAV are mounted on a thrust stand suspended by a brass bar, and the position of the thrust stand is detected by a linear differential transformer. Calibration is performed before and after a series of experiments by applying impulses of known magnitude using small steel balls in an atmospheric–pressure environment. Apparent thrusts, i.e., errors as a result of the pulsed application of axial magnetic fields, are eliminated by measuring the oscillations with a pulsed axial-field application evaluated without main discharges, i.e., in electrically short conditions of the electrodes. The apparent thrusts are less than 3% of the entire measured reaction forces. Thus, the total thrust errors are within 4%. The thrust as a result of arc discharge alone is discussed; i.e., it is yielded by subtracting the thrust caused by cold gas flow from the thrust measured in the arc operation.

Pressure Measurement

To measure the pressure in the discharge chamber, pressure taps are drilled in the cathode tip and in the anode at the same axial position of the cathode tip (Fig. 3a). The pressure probe (Fig. 3b), consists of a piezoelectric pressure transducer and quartz glass tube (2 mm od and 1 mm id), filled with silicon oil. A commercially available transducer (Toyoda PMS-5H), which has both the sensitivity and the rise time required, was selected to capture the rapid transient pressure. Its frequency response is more than 49 kHz. Furthermore, the pressure transducer is electrically insulated from interelectrode plasma by using silicon oil with high viscosity and low compressibility. The measurement errors are within 5%.

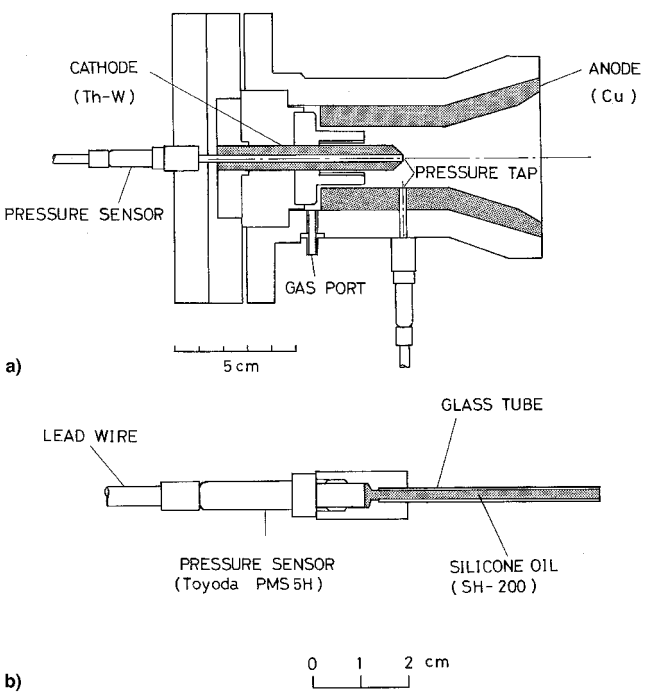

Fig. 3 Configurations of applied-field quasisteady MY-III MPD arcjet for measurement of discharge chamber pressures and pressure probe. Cross sections of a) an MY-III MPD arcjet with pressure probes and b) pressure probes.

Magnetic Probe Measurement

Magnetic flux densities (B_z, B_r, B_θ) are measured independently with three magnetic probes, each of which can detect accurately one component of the magnetic flux density.[8] The probe signals are passively integrated and displayed on a digital oscilloscope. Since the self-field B_θ is proportional to the enclosed current within the radius of the probe position, the distribution of the axial current can be inferred. With the assumption of axial symmetry of the discharge current, the $\dot{B}_\theta$ probe is used to measure the distribution of the local discharge current density (j_z, j_r) in the discharge chamber and near the electrodes. The azimuthal current density j_θ is also inferred using radial and axial components of magnetic flux density. These probes are wound 80 turns with a 40-μm-diam wire on a 1-mm epoxy core. The search coils are encased in a quartz glass tube 2 mm od and 1.7 mm id, and the spacing between the coil and quartz tube is filled with a ceramic material. Probings are performed at intervals of 3 mm along the arcjet axis and 1.5 mm in the radial direction. The magnetic probes are calibrated by the measurement of the magnetic field induced by a known current, which is supplied by the PFN, through a long conductor rod or one-turn coil. The measurement errors are within 4%.

Experimental Results and Discussion

All experimental results shown next are the average of three measurements. The measurements reproducibility was good.

Thruster Performance

It is important to accurately define the limiting discharge current, above which various undesirable effects occur, such as insulator and electrode erosion, and discharge voltage fluctuation. In the present study, J^* is defined as the current at which the discharge voltage waveform changes from a rectangular form to another one. At J^*, the mean-squared deviation of the discharge voltage is 10% of the average voltage over the current pulse of 0.6 ms.

The critical value of $J^2/\dot{m}$ is analytically derived from the rules of Alfvén's critical ionization velocity or minimum input power, and the $J \times B_\theta$ acceleration by the electromagnetic interaction between the discharge current and the azimuthal magnetic field induced by it, as follows[8–11]:

$$J_c^2/\dot{m} = U_c/b = (2e\Phi/M)^{1/2}/b \tag{1}$$

In the present experiments, the mass flow rate is adjusted to 0.40 g/s for H_2, 0.44 g/s for $N_2 + 2H_2$, and 1.37 g/s for Ar, respectively, which corresponds to a J_c of about 10 kA for each propellant species. It is noted that the contribution of acceleration because of the applied magnetic field to Eq. (1), such as swirl and Hall accelerations, is not considered. The acceleration directly caused by the applied magnetic field is treated as an additional component of acceleration in this study.

Figure 4a shows the thrust vs discharge current characteristics for H_2, in which the solid lines marked with MAX and MIN represent the theoretical prediction of electromagnetic acceleration because of the azimuthal self-induced magnetic field as follows:

$$T_m = (\mu/4\pi)J^2[\ell n(r_a/r_c) + \alpha] \tag{2}$$

The anode radius r_a is the value for the cylindrical part of the anode. The quantity α corresponds to 3/4 for the MAX line and 0 for MIN one. Both the closed symbols and characteristic $\otimes$ represent limiting operations at J^*. The application of applied magnetic fields increases the limiting current. Axial-field

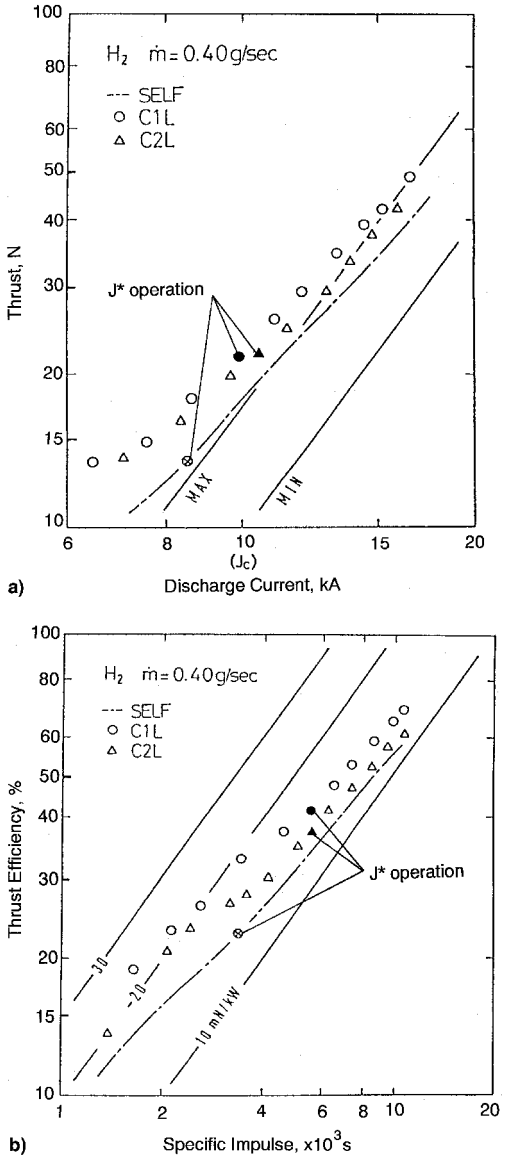

Fig. 4 Thruster performance of a quasisteady MY-III MPD arcjet with applied magnetic fields for H_2 at 0.40 g/s. The performance with only the azimuthal self-field is represented as the symbol SELF. Both the closed symbols and ⊗ represent limiting operations at J^*. All measurement errors are within 4%: a) thrust vs discharge current characteristics and b) thrust efficiency vs specific impulse characteristics.

application increases the thrust at a constant discharge current compared with operation using only the azimuthal self-induced field. The thrust for the C1L-type field is higher than that for the C2L-type field at every discharge current, although the thrust for a low-current, steady-state applied-field thruster increased monotonically with increasing applied magnetic field.[11–14] This cause will be discussed later.

The measured discharge current, voltage, and thrust are used to estimate specific impulse and thrust efficiency through the following relations:

$$I_{sp} = T/\dot{m}g \tag{3}$$

$$\eta = T^2/2\dot{m}VJ \tag{4}$$

$$T_p = T/VJ \tag{5}$$

The thrust efficiencies are plotted as a function of the specific

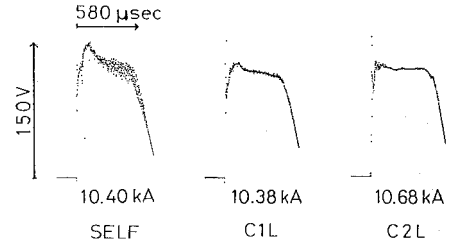

Fig. 5 Voltage waveforms of a quasisteady MY-III MPD arcjet with applied magnetic fields for a mixture of $N_2 + 2H_2$ with 0.44 g/s, around a theoretically predicted critical discharge current of 10 kA.

impulse in Fig. 4b, where solid lines represent theoretical thrust-to-power ratios in units of mN/kW. The thrust efficiency increases at a constant specific impulse under axial-field application. The thrust efficiency for the C1L-type field is larger than that for the C2L-type field at every specific impulse. Stable operations in higher specific impulse levels are achieved for the C1L-type field.

Figure 5 shows the typical waveforms of the discharge voltage for a mixture of $N_2 + 2H_2$ at about 10 kA. The voltage waveform without the axial magnetic field is noisy and somewhat unstable. However, when the axial magnetic field is applied, the voltage fluctuation is not observed at the same discharge currents. Thus, the limiting current with the axial field became greater than that for only the azimuthal self-induced field as shown in Fig. 4a. This fact suggests that axial-field application brings about the reduction of anode erosion because the limiting phenomena are expected to be related closely to formations of current spots on the anode.[8]

Cathode erosion is a significant problem with regard to the lifetime of MPD thrusters.[4,5,17] In Table 1, we summarize the cathode weight loss after discharges of 200–400 shots for a mixture of $N_2 + 2H_2$ at about 10 kA. Cathode loss is defined as the mass loss divided by the total shot number or the integral of current over the discharge duration, which is expressed in microgram per shot and microgram per coulomb, respectively. The measurement errors are within 5%. Table 1 shows that the cathode erosion rate decreases with increasing applied magnetic field strength. It is inferred that the plasma rotating motion caused by the axial magnetic field stabilizes the arc and makes the discharge more uniform; that is, it relaxes the local heating caused by current concentration on the surface of the cathode tip.[2–5,10–12] Furthermore, it will be confirmed later that the current density on the cathode tip decreases as the axial magnetic field strength increases.

From a series of thruster-performance measurements in the high specific impulse range around the theoretically predicted critical current, it is concluded that axial-field application causes the following benefits: 1) an increase in thrust and thrust efficiency, 2) a decrease in electrode erosion, and 3) the achievement of stable operation at high specific impulse levels. These effects almost agree with the previous results measured at low specific impulse levels of 1000–2000 s with large mass flow rates.[2–5] The higher thruster performance was achieved for the C1L-type field than for the C2L-type field. Therefore, considering the influence of axial magnetic field strength and shape on the operational characteristics with both the self-induced and applied magnetic fields, the following guidelines may be obtained to achieve higher thruster performance:

1) The axial magnetic field strength must be smaller than the azimuthal self-field one in the main discharge region near the cathode tip, although electrode erosion decreases with increasing axial-field strength.

2) The applied magnetic field lines must expand gradually downstream for smooth expansion of plasma.[2–7]

Guideline 1 is different from that for low-current, steady-

Table 1 Cathode erosion rates of a quasisteady MY-III MPD arcjet with applied magnetic fields for a mixture of $N_2 + 2H_2$ with 0.44 g/s at about 10 kA

Applied field	Discharge current, kA	Cathode loss, μg/C
SELF	10.2	12.7
C1L	10.0	11.9
C2L	9.8	7.6

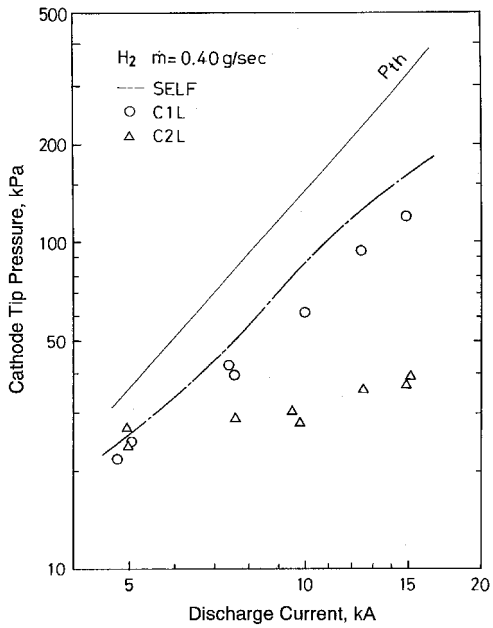

Fig. 6 Pressure on cathode tip vs discharge current characteristics of a quasisteady MY-III MPD arcjet with applied magnetic fields for H_2 at 0.40 g/s. The pressure with only the azimuthal self-field is represented as the symbol SELF. The experimental errors are within 5%.

state thrusters with much stronger applied magnetic fields than the self-induced magnetic fields.

Pressure on Electrodes

The electromagnetic pumping process because of the azimuthal magnetic field induced by the discharge current, is as follows: the radial body force of $-J_z \times B_\theta$ is balanced by a radial gas-pressure gradient in equilibrium; the gasdynamic pressure provides a reaction on the cathode surface. In the idealized model with no axial magnetic field, wherein the entire discharge current enters the end surface of the cylindrical cathode in a uniform normal beam, we obtain the following relation between the pressure on the cathode and the discharge current:

$$P_{\text{th}} = \mu(J/2\pi r_c)^2 \tag{6}$$

Figure 6 shows the pressure on the cathode tip vs discharge current characteristics for H_2. The solid line represents Eq. (6). The pressure on the cathode tip is almost found to be J^2-dependent for only the azimuthal self-induced field and the C1L-type field as predicted from Eq. (6), regardless of propellant species. However, the pressure for the C2L type field does not increase significantly with increasing discharge current. These results agreed with those with a mixture of $N_2 + 2H_2$. For only the azimuthal self-induced field and for the C1L-coil-type field with the smaller axial field strength near the cathode tip than the self-field one (Fig. 2), plasmas are mainly accelerated inward-radially by the electromagnetic interaction between the

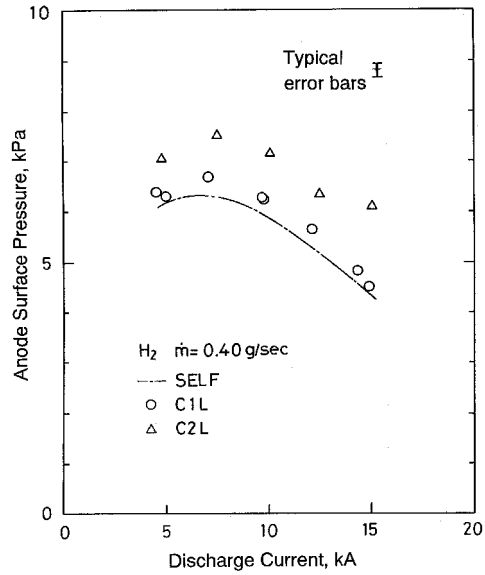

Fig. 7 Pressure on anode vs discharge current characteristics of a quasisteady MY-III MPD arcjet with applied magnetic fields for H_2 at 0.40 g/s. The pressure with only the azimuthal self-field is represented as the symbol SELF.

axial discharge current and the azimuthal self-field. However, for the C2L-type field with the stronger axial magnetic field, plasma is rotated by the azimuthal electromagnetic force, which is generated by the interaction between the axial magnetic field and the radial discharge current.[9–12] The generated centrifugal force decreases the pressure on the cathode. As a result, the pumping thrust on the cathode decreases with increasing axial magnetic field strength at a constant discharge current in the present experimental conditions, with both the self-induced and applied magnetic fields. Therefore, the overall thrust for the C2L-type field measured as shown in Fig. 4a, is lower than that for the C1L-type field, although additional thrusts directly caused by the axial magnetic field, such as those from swirl and Hall accelerations, increases with increasing axial magnetic field strength.

Figure 7 shows the pressure on the anode vs discharge current characteristics for H_2. For the self-induced magnetic field, the pressure on the anode has a maximum at a discharge current of about 7 kA with increasing discharge current. This behavior is also observed for the C1L- and C2L-coil-type fields. This is expected because of conflicting effects of increased thermalization and electromagnetic acceleration with increasing discharge current.[2–5] The pressure on the anode becomes large at a constant discharge current as the axial magnetic field strength increases. This result agrees with the limiting current increasing with the axial field strength (Fig. 4a), because the shortage of current carrier is expected to be relaxed near the anode. This is expected because of the existence of the centrifugal force under axial-field application, as well as the pressure characteristics on the cathode, as described earlier.

Current Distributions

The enclosed discharge current contours measured for H_2 at about 10 kA are drawn in Fig. 8, where the numbers on the contours indicate the fractions of the current downstream of the given line to the discharge current. Compared with the contours for only the azimuthal self-induced magnetic field and for the C1L-coil-type field, the current contours for the C2L-coil-type field are withdrawn more upstream in the discharge chamber, although those for a mixture of $N_2 + 2H_2$ moved upstream, even for the C1L-type field.[6] This is expected because thermalization is enhanced owing to the rotation motion

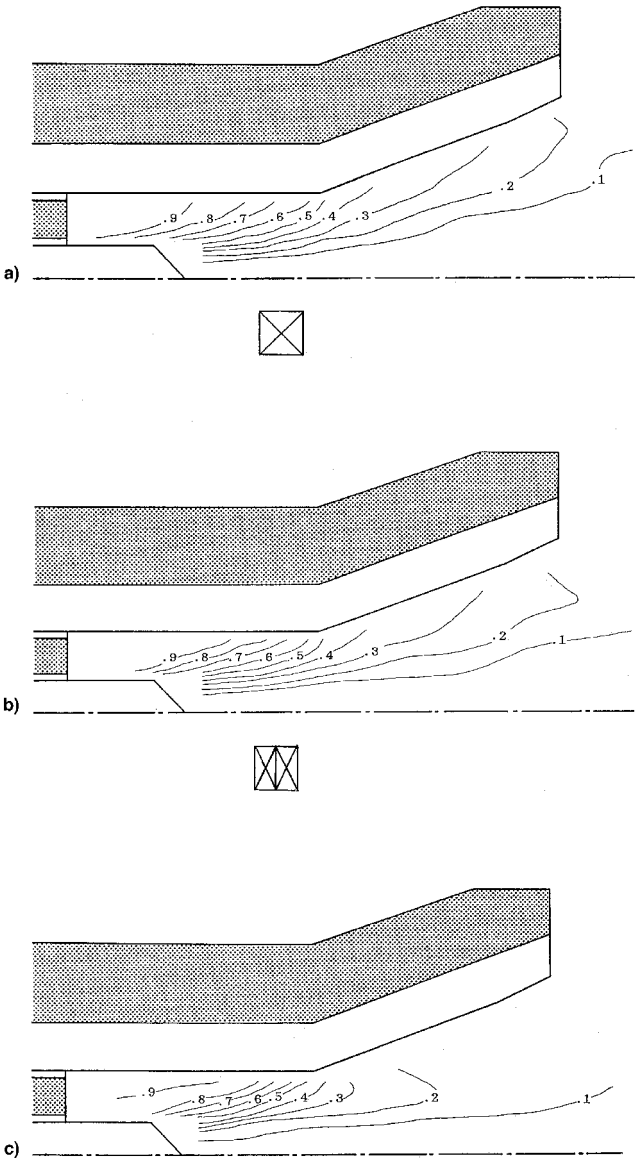

Fig. 8 Discharge current distributions in a quasisteady MY-III MPD arcjet with applied magnetic fields for H_2 with 0.40 g/s at 10 kA. The measurement errors are within 4%: a) only azimuthal self-field, b) C1L-type field, and c) C2L-type field.

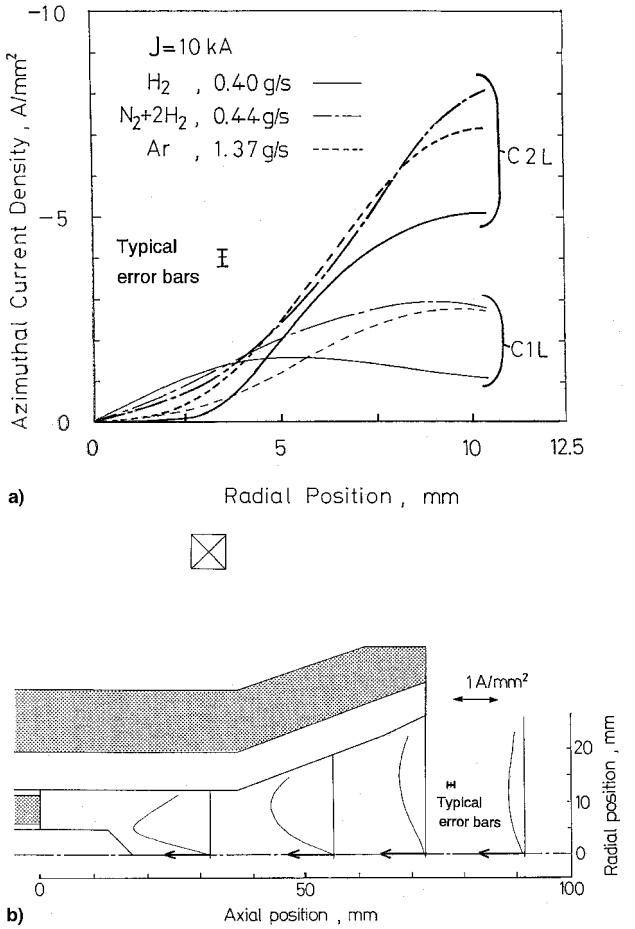

Fig. 9 Azimuthal current patterns of a quasisteady MY-III MPD arcjet with applied magnetic fields for H_2, mixture of $N_2 + 2H_2$, and Ar at 10 kA. Radial profiles of azimuthal current density a) for C1L- and C2L-type fields with various gases in axial position of ring coil and b) for a C1L-type field with H_2 in various axial positions.

of electrons under axial-field application.[2-5] Accordingly, the discharge current with the axial magnetic field flows in an active region with a large electron density and a high electron temperature, and the propellant gas is expected to be heated more efficiently.[7]

In addition, an increase in the axial magnetic field strength is found to decrease the current fraction on the cathode tip. This is related closely to the reduction of cathode erosion under axial-field application. The pumping pressure at the cathode tip because of the electromagnetic interaction between the azimuthal self-induced magnetic field and the axial discharge current can be estimated from the measured current fraction on the cathode. For the C2L-type field, the estimated pumping pressure is much larger than that measured with the pressure probe, as shown in Fig. 6. Therefore, an additional outward-radial force as a direct result of the applied axial magnetic field, such as the centrifugal force caused by the $-J_r \times B_z$ rotating motion, is expected to exist with the strong axial field, as inferred earlier.

Figure 9 shows the radial variations of the azimuthal current density at 10 kA in the MY-III MPD arcjet chamber. As shown in Fig. 9a, the azimuthal current densities, which are expected to be Hall currents, at an axial position of the ring coil become larger with increasing radius, except with H_2 for the C1L-type field. These azimuthal current densities are almost constant near the anode surface. The azimuthal currents for the C2L-type field are higher than those for the C1L-type field above a radius of about 5 mm, regardless of gas species. As seen in Fig. 9b, the azimuthal current for the C1L-type field, with H_2, has a maximum for radial variation at a constant axial position. For example, at the axial location of the ring coil, the azimuthal current density takes a maximum of 160 A/cm^2 at a radius of 5 mm, which equals the radius of the cathode corner. This result is likely correlated with the radial current density, as shown in Fig. 8, and the axial field strength. The maximum value is higher at the more upstream region because the applied magnetic field is stronger near the ring coil along the axis. The axial magnetic field induced by the azimuthal current is in the reverse direction of the external magnetic field applied by the ring coil. The azimuthal current generates the electromagnetic force $-J_\theta \times B_r$ in the axial direction, which is called Hall acceleration.[15,16] Using the obtained data, the thrust because of Hall acceleration is evaluated to be less than 1 N. Therefore, it is concluded that Hall acceleration is not the main mechanism of additional-thrust generation under the present axial-field application.

Thrust Components

Thrust components are estimated from the following methods[6,9,10-12,16]:

Table 2 Thrust components of a quasisteady MY-III MPD arcjet with applied magnetic fields for H_2 with 0.40 g/s at about 10 kA

Applied field	Electromagnetic: Blowing, T_b(N)[a]	Electromagnetic: Pumping, T_p(N)[b]	Electromagnetic: Hall, T_h(N)[a]	Electrothermal, T_r(N)[b]	$T = T_b + T_p + T_h + T_r$ N	Total thrust,[c] N
SELF[d]	12.7	3.2	0.0	2.7	18.6	17.8
C1L	12.3	2.0	0.2	3.1	17.6	22.0
C2L	11.1	0.8	0.8	3.5	16.2	20.6

[a]Inferred from the magnetic field probing.
[b]Inferred from the pressure measurements near the electrodes.
[c]Measured by the pendulum method.
[d]The thrust components with only the azimuthal self-field is represented as the symbol SELF.

1) The total thrust, as shown in Fig. 4a, is measured by the pendulum method.

2) The electromagnetic blowing thrust, caused by the axial body force of $J_r \times B_\theta$, is evaluated from the measured azimuthal self-induced magnetic field and radial current shown in Fig. 8.

3) The electromagnetic pumping thrust, which is expected because of the radial body forces of $-J_z \times B_\theta$ and $J_\theta \times B_z$, and because of the centrifugal force caused by the $-J_r \times B_z$ rotating motion, is evaluated from the measured pressure on the cathode tip shown in Fig. 6.

4) The thrust of Hall acceleration caused by the axial body force of $-J_\theta \times B_r$ is evaluated from the measured radial magnetic field and azimuthal current shown in Fig. 9.

5) The electrothermal thrust, which reacts on the inside surface of the discharge chamber, is roughly inferred from the measured pressure on the anode shown in Fig. 7.

Table 2 summarizes the estimated electromagnetic, electrothermal, and total thrusts for H_2 at about 10 kA. The sum of the estimated thrust components for only the azimuthal self-field exceeds the total thrust measured by the pendulum method. This is expected because the electrothermal thrust for only the self-field is overestimated. However, the sums of the thrust components for the applied axial fields are found to be smaller than the total thrusts measured by the pendulum method. Under axial-field application, additional thrusts, which are expected to be a direct result of the axial magnetic field, contribute to the total thrust. Because the thermalization enhanced in the axial magnetic field contributes very little to the thrust in the high specific impulse operations, the mechanism of additional-thrust generation is mainly expected to be swirl acceleration with a strong centrifugal force, as predicted in Ref. 16. However, the additional thrust of 4.4 N for the C1L-type field equals that for the C2L-type field, and the cause is unknown.

Conclusions

The quasisteady magnetoplasmadynamic arcjet with applied axial magnetic fields was operated in high specific impulse levels around a critical discharge current predicted from the rules of Alfvén's ionization velocity or minimum input power, to improve the thruster performance and understand the complex acceleration mechanisms with both the self-induced and applied magnetic fields. The application of axial magnetic fields was found to achieve higher thrust efficiencies than those for only the self-induced magnetic field at constant specific impulses and to achieve stable operations at higher specific impulses with less electrode erosion. However, performance decreased at a constant discharge current when the axial magnetic field strength exceeded the azimuthal self-field one near the cathode tip, in contrast to results for a low-current steady-state applied-field thruster with a negligible self-field, for which the thrust increased with increasing axial magnetic field strength. As the axial field strength increased, the pressures on the cathode tip and the anode decreased and increased, respectively, at a constant discharge current. The discharge current flowed more upstream in the discharge chamber with increasing axial field strength, and the azimuthal current became larger when approaching the ring coil. The measured pressures on the electrodes and the current distributions showed that the overall thrust measured by the pendulum method increased, in spite of a decrease in the electromagnetic pumping thrust and a small contribution of Hall acceleration. Thus, an additional thrust component as a direct result of the axial magnetic field, such as that caused by swirl acceleration, is expected to exist.

References

[1]Toki, K., Shimizu, Y., Kuriki, K., Suzuki, H., and Kunii, Y., "Development of an MPD Thruster System for the EPEX Space Test," *Proceedings of the 23rd International Electric Propulsion Conference*, Vol. 1, Electric Rocket Propulsion Society, 1993, pp. 554–561 (Paper IEPC-93-058).

[2]Tahara, H., Kagaya, Y., and Yoshikawa, T., "Quasi-Steady MPD Arcjets with Applied Magnetic Fields," AIAA Paper 85-2001, Oct. 1985.

[3]Tahara, H., Kagaya, Y., and Yoshikawa, T., "Hybrid MPD Thruster with Axial and Cusp Magnetic Fields," *Proceedings of the 20th International Electric Propulsion Conference*, Electric Rocket Propulsion Society, 1988, pp. 333–341 (Paper IEPC-88-058).

[4]Yoshikawa, T., Kagaya, Y., Tahara, H., and Wasa, T., "Continuous Operation of a Quasi-Steady MPD Propulsion System with an External Magnetic Field," *Proceedings of 20th International Electric Propulsion Conference*, Electric Rocket Propulsion Society, 1988, pp. 315–322 (Paper IEPC-88-056).

[5]Tahara, H., Kagaya, Y., and Yoshikawa, T., "Quasisteady Magnetoplasmadynamic Thruster with Applied Magnetic Fields for Near-Earth Missions," *Journal of Propulsion and Power*, Vol. 5, No. 6, 1989, pp. 713–717.

[6]Tahara, H., Sasaki, M., Kagaya, Y., and Yoshikawa, T., "Thruster Performance and Acceleration Mechanisms of a Quasi-Steady Applied-Field MPD Arcjet," AIAA Paper 90-2554, July 1990.

[7]Tahara, H., Kagaya, Y., and Yoshikawa, T., "Effects of Applied Magnetic Fields on Performance of a Quasisteady Magnetoplasmadynamic Arcjet," *Journal of Propulsion and Power*, Vol. 11, No. 2, 1995, pp. 337–342.

[8]Tahara, H., Yasui, H., Kagaya, Y., and Yoshikawa, T., "Experimental and Theoretical Researches on Arc Structure in a Self-Field Thruster," AIAA Paper 87-1093, May 1987.

[9]Malliaris, A. C., "Phenomena in the Cathode Region of an MPD Accelerator," *AIAA Journal*, Vol. 5, No. 7, 1967, pp. 1325–1328.

[10]Patrick, R. M., and Schneiderman, A. M., "Performance Characteristics of a Magnetic Annular Arc," *AIAA Journal*, Vol. 4, No. 2, 1966, pp. 283–290.

[11]Nerheim, N. M., and Kelly, A. J., "A Critical Review of the Magnetoplasmadynamic (MPD) Thruster for Space Application," California Inst. of Technology, Jet Propulsion Lab., TR 32-1196, Pasadena, CA, Feb. 1968.

[12]Fradkin, D. B., Blackstock, A. W., Roehling, D. J., Stratton, T. F., Williams, M., and Liewer, K. W., "Experiments Using a 25-kW Hollow Cathode Lithium Vapor MPD Arcjet," *AIAA Journal*, Vol. 8, No. 5, 1970, pp. 886–894.

[13]Myers, R. M., "Applied-Field MPD Thruster Performance with Hydrogen and Argon Propellants," *Journal of Propulsion and Power*,

Vol. 9, No. 5, 1993, pp. 781–784.

[14]Myers, R. M., "Geometric Scaling of Applied-Field Magnetoplasmadynamic Thrusters," *Journal of Propulsion and Power*, Vol. 11, No. 2, 1995, pp. 343–350.

[15]Sasoh, A., and Arakawa, Y., "Electromagnetic Effects in an Applied-Field MPD Thruster," *Journal of Propulsion and Power*, Vol. 8, No. 1, 1992, pp. 98–102.

[16]Sasoh, A., and Arakawa, Y., "Thrust Formula for Applied-Field Magnetoplasmadynamic Thrusters Derived from Energy Conservation Equation," *Journal of Propulsion and Power*, Vol. 11, No. 2, 1995, pp. 351–356.

[17]Mantenieks, M. A., and Myers, R. M., "Component Erosion in 100-kW Class Applied-Field, Water-Cooled MPD Thrusters," *Proceedings of the 23rd International Electric Propulsion Conference*, Vol. 2, Electric Rocket Propulsion Society, 1993, pp. 1100–1123 (Paper IEPC-93-121).